Steady Wind-driven Upwelling in the Presence of a Baroclinic Coastally Trapped Jet*

A. E. HAY AND E. D. KINSELLA

Department of Physics and Newfoundland Institute for Cold Ocean Science, Memorial University of Newfoundland, St. John's, Newfoundland, Canada

(Manuscript received 18 October 1984, in final form 30 December 1985)

ABSTRACT

The usual two-layer model for steady wind-driven upwelling along a uniform coastline is extended to incorporate the effects of an upper-layer jet trapped against the coast. The characteristic width of the jet is the internal deformation radius, so the jet Rossby number in the governing equations for the upper layer is order of unity, and the nonlinear term involving cross-stream shear must be retained. It is shown, however, that the equations can be reduced to a manageable form when the upper-layer thickness and equilibrium displacement of the interface are both much less than the total depth. Explicit solutions are obtained for equilibrium jet profiles for which the interface is either exponential, which corresponds to a frictionless jet with uniform potential vorticity, or parabolic. It is also shown that solutions should be obtainable when the jet profile can be expressed as an arbitrary polynomial in the offshore coordinate. The principal differences between our results and the usual ones for the no-jet case are that upwelling is reduced at the coast and amplified offshore. The differences are due to a reduction in the divergence of the on–offshore velocities within an internal Rossby radius of the coast and to increased divergence farther offshore. These changes in divergence are the result of the equilibrium displacement of the interface through the continuity equation and of advection of mean flow momentum by wind-induced offshore motion through the cross-stream shear.

1. Introduction

The problem of coastal upwelling in the presence of a jet with finite Rossby number does not appear to have been previously addressed in the literature. Niiler (1969) investigated the effect of a free barotropic jet on the depth-dependent Ekman layer solution and concluded that upwelling should occur along the jet axis for a wind stress directed parallel to the mean flow. This effect was ascribed to a reduction in the effective Coriolis parameter at the jet axis owing to the large cross-stream shear. The shear enters the problem through the nonlinear advective term in the momentum equations. Advection of mean flow momentum by wind-induced velocities is also investigated here. There are three principal points of departure from Niiler's work. First, instead of a free barotropic jet a two-layer system is considered, with the jet trapped against an infinite coastline. Second, the time-dependent local acceleration in the longshore direction is included. Third, the equations of motion are vertically integrated in each layer rather than retaining the depth dependence through an eddy-viscosity parameterization of the vertical turbulent momentum fluxes. The present investigation therefore represents an extension of the usual two-layer coastal upwelling model to include the effects of cross-stream advection by wind-induced perturbation velocities on the momentum balance, and the effects of the equilibrium displacement of the interface on the vertically integrated mass and momentum conservation equations.

The motivation for the study arose from our interest in the possible effects of the Labrador Current on wind-driven upwelling at the edge of the Labrador Shelf and the Grand Bank. This current flows southward with shallow water to its right, and the underlying isopycnals therefore plunge downward toward the shelf. Typical temperature, salinity and σ_t sections are shown in Fig. 1. These sections extend along a line at 45°10′N from the Grand Bank across the shelf break over the slope. The Labrador Current is clearly evident as the core of cold water spanning the shelf break. To seaward of the shelf break and below the low-temperature core, isopleths of all three scalar quantities plunge downward in the direction of the shelf. The flow is directed from north to south, with shallow water to the right. Upwelling-favorable winds, however, are directed in the sense opposite to that of the current, since the shallow water must be to the left of the wind. A typical value for the Rossby number can be estimated using a cross-stream length scale $L_0 \sim 25$ km (Fig. 1) and typical mean speeds $u_0 \sim 50$ cm s^{-1} (Petrie and Anderson, 1983), giving $u_0/fL_0 \sim 0.2$. While this value is not large, neither is it small, and the possible importance of nonlinear effects cannot be ignored a priori. This then is the physical system in which we are ultimately interested. As a first step, however, we have chosen to ex-

* Newfoundland Institute for Cold Ocean Science Contribution No. 71.

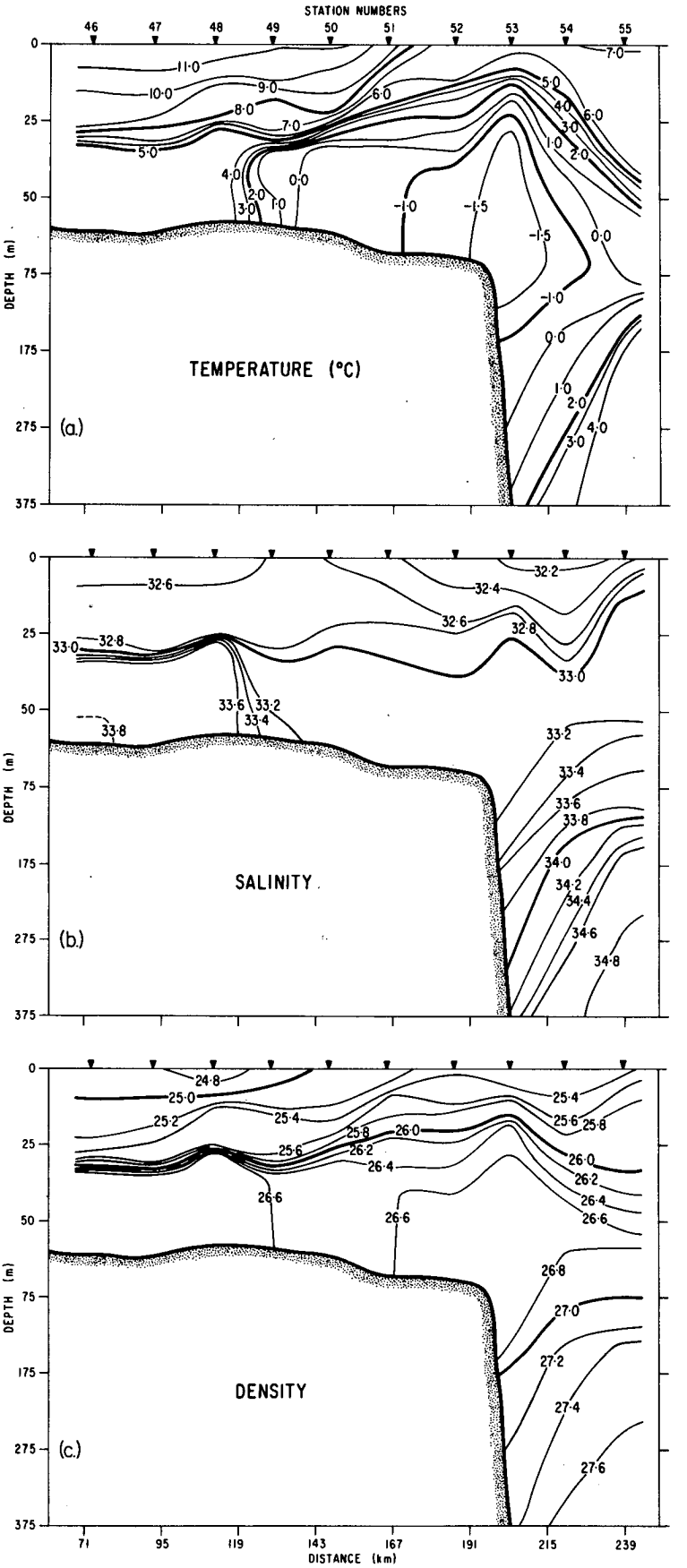
STATION NUMBERS
46
47
48
49
50
51
52
53
54
55
DEPTH (m)
0
25
50
75
175
275
375
TEMPERATURE (°C)
(a.)
11·0
10·0
9·0
8·0
7·0
6·0
5·0
4·0
3·0
2·0
1·0
0·0
-1·0
-1·5
7·0
6·0
5·0
4·0
3·0
2·0
1·0
0·0
-1·0
-1·5
0·0
1·0
2·0
3·0
4·0
SALINITY
(b.)
32·6
32·8
33·0
33·2
33·4
33·6
33·8
32·2
32·4
32·6
32·8
33·0
33·2
33·4
33·6
33·8
34·0
34·2
34·4
34·6
34·8
DENSITY
(c.)
24·8
25·0
25·2
25·4
25·6
25·8
26·0
26·2
26·4
26·6
25·4
25·6
25·8
26·0
26·2
26·4
26·6
26·8
27·0
27·2
27·4
27·6
71
95
119
143
167
191
215
239
DISTANCE (km)

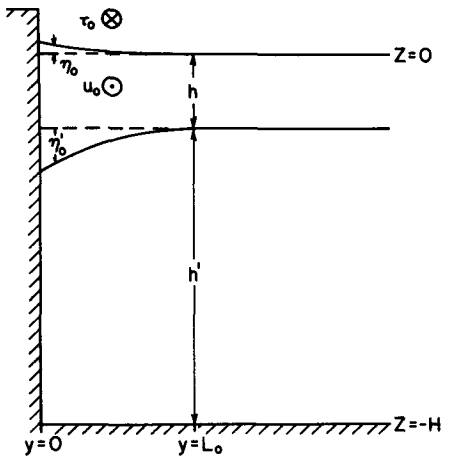

FIG. 2. Sketch of an upper-layer, coastally trapped jet. The x-coordinate is positive into the page; the y-coordinate positive to the left.

amine the simpler problem of upwelling in the presence of a jet trapped at the coast rather than at the shelf break.

2. Formulating the problem for the baroclinic response

Consider the two-layer representation of a coastally trapped upper-layer jet in Fig. 2. The alongshore coordinate is x, the offshore coordinate y. Prior to the onset of the wind stress, the undisturbed jet flows in the $+x$ direction with speed $u_0(y)$ and $v_0 = 0$. The lower layer is assumed to be at rest initially. All parameters are taken to be independent of alongshore distance. The wind stress at the sea surface, $-\tau_0$, is initiated at time $t = 0$, spatially uniform, and directed alongshore in the sense opposite to that of the jet. Interfacial and bottom stresses are ignored.

Making the hydrostatic approximation, the horizontal momentum equations for the upper layer are

$$u_t + vu_y - fv = \frac{1}{\rho}\tau_z^x \tag{1}$$

$$v_t + fu = -g\eta_y. \tag{2}$$

The subscripts denote partial differentiation. The vu_y term is the only nonlinear term retained, anticipating that cross-stream advection of downstream momentum will be important. In the lower layer,

$$u'_t - fv' = 0 \tag{3}$$

$$v'_t + fu' = -g\eta_y - g'\eta'_y \tag{4}$$

where primes have been used to denote lower-layer quantities, and $g' = g(\rho' - \rho)/\rho$. The vertically integrated continuity equations in each layer are

$$(\eta - \eta')_t + [(h + \eta - \eta')\bar{v}]_y = 0 \tag{5}$$

$$\eta'_t + [(h' + \eta')\bar{v}']_y = 0 \tag{6}$$

where the overbar denotes the vertical average. These equations differ from the usual two-layer upwelling equations for an infinite coastline because of the nonlinear term in (1).

We define zero-order quantities (u_0, η_0, η'_0) which characterize the initial state, and perturbation quantities ($\tilde{u}$, $\tilde{v}$, $\tilde{u}'$, $\tilde{v}'$, $\tilde{\eta}$, $\tilde{\eta}'$), and substitute $u = u_0 + \tilde{u}$, $\eta = \eta_0 + \tilde{\eta}'$, $v = \tilde{v}$ etc. in (1) to (6). In the unperturbed state these equations reduce to

$$\left.\begin{aligned} fu_0 &= -g\eta_{0y} \\ g\eta_{0y} &= -g'\eta'_{0y} \end{aligned}\right\}.$$

Retaining only those terms that are first order in perturbation quantities, and vertically integrating over each layer gives, for the upper layer,

$$\tilde{u}_t + \tilde{v}u_{0y} - f\tilde{v} = \frac{\tau}{\rho(h - \eta'_0)} \tag{7a}$$

$$\tilde{v}_t + f\tilde{u} = -g\tilde{\eta}_y \tag{7b}$$

$$[(h - \eta'_0)\tilde{v}]_y = \tilde{\eta}'_t \tag{7c}$$

in which $\tau = -\tau_0$ is the wind stress, and for the lower layer,

$$\tilde{u}'_t - f\tilde{v}' = 0 \tag{8a}$$

$$\tilde{v}'_t + f\tilde{u}' = -g'\tilde{\eta}'_y - g\tilde{\eta}_y \tag{8b}$$

$$[(h' + \eta'_0)\tilde{v}']_y = -\tilde{\eta}'_t. \tag{8c}$$

The rigid-lid approximation has been used, since we are interested in the baroclinic response, and it has been assumed that η_0, $\tilde{\eta}$ and $\tilde{\eta}' \ll \eta'_0$ in the continuity equations. It is understood that $\tilde{u}$ and $\tilde{v}$ represent the vertically averaged perturbation velocity components. Henceforth, the tildes will be dropped for convenience.

The horizontal momentum equations can be reduced to

$$v'_{tt} + f^2v' - g'[(h' + \eta'_0)v']_{yy} = v_{tt} - fvu_{0y} + f^2v + \frac{f\tau}{\rho(h - \eta'_0)} \tag{9}$$

in which use has been made of (8c). A steady solution is sought, so v_{tt} and v'_{tt} are dropped. This requirement

FIG. 1. Temperature, salinity and density (σ_t) sections across the Labrador Current. Note the change in vertical scale at 75 m depth. These data were acquired on 24 June 1983 along a transect extending from west to east across the shelf break at 45°10′N. The reader is referred to Hill et al. (1975) and Smith et al. (1937) for more extensive but lower-resolution sections across the Labrador Current at the edge of the Grand Bank.

supposes that a time of at least $O(f^{-1})$ has passed since the onset of the wind stress (Gill, 1982, p. 396). Since v and v' vanish at the coast, (7c) and (8c) require that

$$(h - \eta_0')v = -(h' + \eta_0')v' \tag{10}$$

and substitution in (9) gives

$$[f^2 - g'\eta_{0yy}']v' - g'\left(\frac{h - \eta_0'}{H}\right) \times [2\eta_{0y}'v_y' + (h' + \eta_0')v_{yy}'] = \frac{f\tau}{\rho H} \tag{11}$$

with $H = h + h'$ and $fu_{0y} = g'\eta_{yy}'$.

We now estimate the relative importance of the different terms on the left-hand side of (11). Let L_0 represent the offshore length scale of the unperturbed jet. We are interested in those cases for which the jet Rossby number $u_0/fL_0 \sim O(1)$. Letting $\hat{\eta}_0'$ be the magnitude of the interfacial displacement at $y = 0$, we find that

$$L_0^2 \approx \frac{g'}{f^2}\hat{\eta}_0'. \tag{12}$$

Now, let L be the offshore length scale of the baroclinic upwelling response. In the absence of the jet, this is just the internal Rossby radius

$$a'^2 = g'\frac{hh'}{H}. \tag{13}$$

We assume that $L \sim a'$ even in the presence of a jet. In this case we find that

$$\frac{2\eta_{0y}'v_y'}{(h' + \eta_0')v_{yy}'} \approx \frac{2\hat{\eta}_0'}{(h' + \eta_0')}\frac{L}{L_0} \approx 2\left(\frac{h\hat{\eta}_0'}{Hh'}\right)^{1/2} \ll 1$$

provided that

$$|\hat{\eta}_0'| \ll h' \tag{14a}$$

$$h \ll H. \tag{14b}$$

Under these conditions the $\eta_{0y}'v_y'$ term in (11) may be ignored. The ratio of the remaining terms is

$$\frac{(f^2 - g'\eta_{0yy}')v'H}{g'(h - \eta_0')(h' + \eta_0')v_{yy}'} = \frac{2hh'}{(h - \eta_0')(h' + \eta_0')}$$

which, given (14a), is O(1) for $\eta_0' < 0$. Under these conditions, (11) takes the form

$$[f^2 - g'\eta_{0yy}']v' - \frac{g'h'}{H}(h - \eta_0')v_{yy}' = \frac{f\tau}{\rho H}. \tag{15}$$

Note that the presence of the jet has resulted in two terms that do not occur in the equation equivalent to (15) in the usual two-layer model. One is the $g'\eta_{0yy}'$ term, which results from cross-stream shear through the nonlinear term in (7a); the other is the $-\eta_0'$ term, which arises from the equilibrium deformation of the interface through the continuity equation.

It is convenient to define the nondimensional variables

$$\gamma = y/a' \tag{16}$$

$$\psi_0 = \eta_0'/h. \tag{17}$$

Substitution in (15) gives

$$(1 - \psi_0)v_{\gamma\gamma}' - \left(1 - \frac{H}{h'}\psi_{0\gamma\gamma}\right)v' = -\frac{\tau}{\rho f H}. \tag{18}$$

If ψ_0 is set to zero, this reduces to the usual result in the absence of a jet.

Equation (18), and its alternate (15), form the basis for the rest of the discussion. Reiterating, these equations govern the baroclinic upwelling response for a jet with Rossby number O(1) and which satisfies the conditions (14a) and (14b). From (18) it is clear that the solutions depend on the choice of jet profile, ψ_0. In the following we show that solutions are possible for at least two types of profile and then give explicit results for specific instances of each.

We first note that a special class of solutions to (18) exists if

$$\psi_0 = \hat{\psi}_0 \exp\left[-\left(\frac{h'}{H}\right)^{1/2}\gamma\right]. \tag{19}$$

In this case (18) becomes

$$v_{\gamma\gamma}' - v' = -\frac{\tau}{\rho f H[1 - \psi_0(\gamma)]} \tag{20}$$

which is readily solved.

Another class of solutions exists if ψ_0 can be represented by a polynomial in γ. If we let

$$\psi_0 = \hat{\psi}_0 + b_1(1 - \hat{\psi}_0)\gamma + b_2(1 - \hat{\psi}_0)\gamma^2 + \cdots \tag{21}$$

and use the Frobenius method (e.g., Hildebrand 1962, p. 129) with

$$v' = \sum_{k=0}^{\infty} a_k\gamma^{k+s}, \tag{22}$$

then it can be shown that there are in general two linearly independent solutions of the form (22), one with $s = 0$, the other with $s = 1$.

3. Coastally trapped jet with uniform potential vorticity

We choose for the purpose of illustration a jet for which the potential vorticity is invariant with offshore distance. The reason for this choice will become apparent, but it is of sufficient oceanographic interest in any case. For example, Stommel (1965, pp. 108–109) showed that the potential vorticity is nearly uniform across the Gulf Stream, and Griffiths et al. (1982) have assumed uniform potential vorticity in an investigation of instabilities in baroclinic jets.

Equating the potential vorticities in each layer to their values, f/h and f/h', outside the jet region, the following relations are found:

$$-u_{0y} = \frac{f}{h}(\eta_0 - \eta_0') \tag{23}$$

$$-u_{0y}' = \frac{f}{h'}\eta_0' \tag{24}$$

where $-u_{0y}$ and $-u_{0y}'$ are the relative vorticities in the upper and lower layers, respectively, and f is assumed constant. Defining the difference velocity $\delta \equiv u_0 - u_0'$, and making the approximation $\eta_0 \ll \eta_0'$, we find from (23) and (24) that

$$\delta_y = \frac{fH}{hh'}\eta_0'.$$

A second expression, $\delta_y = g'\eta_{0yy}'$, can be obtained from the geostrophic relations for the upper and lower layers, and combining the two gives

$$\eta_0' = a'^2\eta_{0yy}'.$$

The profile of a jet with uniform potential vorticity, bounded by a coastline at $y = 0$ to the right of the mean flow direction, is therefore

$$\eta_0' = -\hat{\eta}_0' e^{-y/a'} \tag{25}$$

where $\hat{\eta}_0' > 0$. This exponential profile compares favorably with the isopycnals at the base of the Labrador Current in Fig. 1 ($\sigma_t = 27.2$ for example).

4. Solutions for the baroclinic response

a. *Exponential profile*

Comparing (19) and (25) it is seen that the two are nearly identical for the case of interest, $h \ll H$ (Eq. 14b). We therefore rewrite (20) in the form

$$v_{\gamma\gamma}' - v' = \frac{-\tau}{\rho fH(1 + a_* e^{-\gamma})} \tag{26}$$

where $a_* = -\hat{\psi}_0 = \hat{\eta}_0/h$. The solution of (26) is

$$v' = \frac{\tau e^{-\gamma}}{\rho fHa_*}\int_0^\gamma e^{2\zeta}\ln(1 + a_* e^{-\zeta})d\zeta. \tag{27}$$

Using (8c) and making no further approximations, we have

$$\eta' = \frac{-\tau t}{\rho fa'}\frac{h'}{H}\left[\left(\frac{h' + \eta_0'}{h'}\right)\frac{e^\gamma}{a_*}\ln(1 + a_* e^{-\gamma}) - \left(\frac{h' + 2\eta_0'}{h'}\right)\frac{e^{-\gamma}}{a_*}\int_0^\gamma e^{2\zeta}\ln(1 + a_* e^{-\zeta})d\zeta\right]. \tag{28a}$$

For cases satisfying (14a), this becomes

$$\eta' \approx \frac{-\tau t}{\rho fa'}\frac{h'}{H}\left[\frac{e^\gamma}{a_*}\ln(1 + a_* e^{-\gamma}) - \frac{e^{-\gamma}}{a_*}\int_0^\gamma e^{2\zeta}\ln(1 + a_* e^{-\zeta})d\zeta\right]. \tag{28b}$$

The integral in these equations is given by

$$\int_0^\gamma e^{2\zeta}\ln(1 + a_* e^{-\zeta})d\zeta = \frac{1}{2}\left[e^{2\gamma}\ln(1 + a_* e^{-\gamma}) - \ln(1 + a_*) + a_*^2\ln\left(\frac{1 + a_*}{1 + a_* e^{-\gamma}}\right) - a_*^2\gamma + a_*(e^\gamma - 1)\right]. \tag{29}$$

The solution for v can be obtained using (10).

These results are to be compared with the usual ones for upwelling in the absence of a jet (e.g., Csanady 1982, p. 89):

$$v' = \frac{\tau}{\rho fH}(1 - e^{-\gamma}) \tag{30a}$$

$$\eta' = \frac{-\tau t}{\rho fa'}\frac{h'}{H}e^{-\gamma} \tag{30b}$$

which can be obtained from (26) with $a_* = 0$, or from (27) and (28) in the limit $a_* \to 0$.

The results for v' normalized by $\tau_0/\rho fH$ and η' normalized by $\tau_0 th'/\rho fa'H$ are shown in Fig. 3 for $a_* = 0.9$. It is seen that the flow toward the coast is everywhere reduced in the presence of the jet, and that the upwelling rate is 27% lower at the coast, but enhanced at distances $\geq a'$ from shore. Since the approximate form of (28) is identical to the result which would be obtained if η_0' were set to zero in the continuity equation (8c), it is clear that the enhanced upwelling beyond $y = a'$ in Fig. 3b is entirely due to the greater divergence of the on–offshore velocities in this region (Fig. 3a).

This point is underscored by an analysis of the behavior of the solutions as a function of a_*, which we present now. From (28a) the interfacial displacement at the coast is given by

$$\hat{\eta}'\left[\frac{\tau_0 th'}{\rho fa'H}\right]^{-1} = \frac{1}{a_*}\ln(1 + a_*). \tag{31}$$

In the limit $a_* \to 0$, this tends to unity, as required [see Eq. (30b)]. For a_* very large, upwelling at the coast is effectively reduced to zero in the presence of the jet. The sensitivity of $\hat{\eta}'$ to a_* is largest, however, for small values of a_*, $d\hat{\eta}'/da_*$ being a maximum at $a_* = 0$.

The normalized values of v', v and η' are plotted in Fig. 4 for values of a_* ranging from 0 to 100: v' and η' are normalized as in Fig. 3, v by $\tau_0 h'/(\rho fHh)$. Figure 4c illustrates the suppression of upwelling rates at the coast. This is clearly associated with large reductions in the divergence of v' (Fig. 4a). Perhaps the most remarkable feature of these solutions, however, is the prediction that a second upwelling zone develops at distances $y > a'$ for $a_* \geq 5$. Maximum upwelling rates in this zone are relatively independent of a_*, but exceed those at the coast for a_* large enough. The maximum upwelling rate occurs where the divergence of v' is a

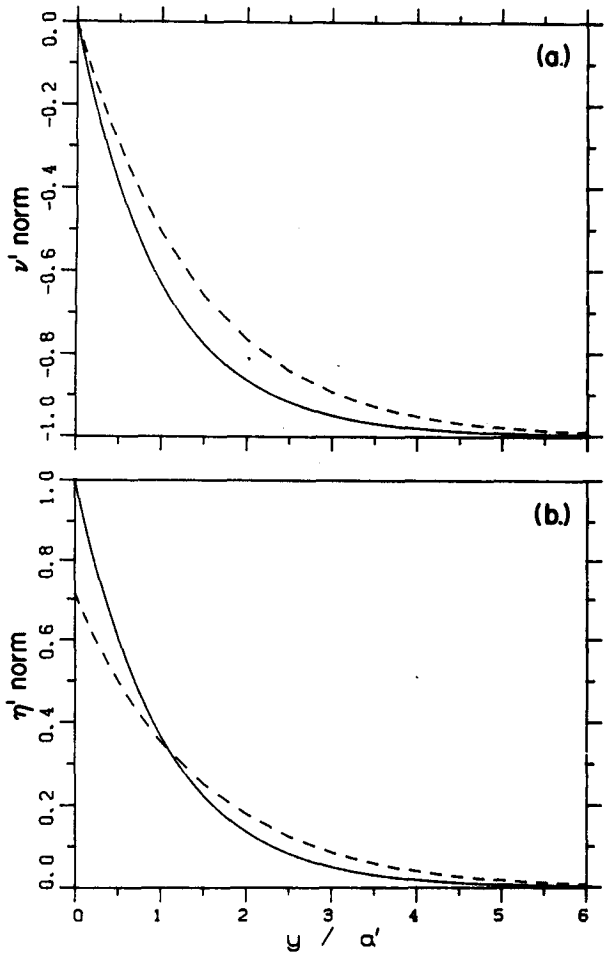

FIG. 3. Exponential case. (a) Lower-layer velocities and (b) interfacial displacements, normalized as indicated in the text. The solid line is the usual (no-jet) solution; the dashed line the solution in the presence of a jet.

maximum (Fig. 4a). This behaviour is discussed further in a later section.

b. Parabolic profile

We now consider the class of solutions in which the jet profile can be represented by a polynomial in y. We choose a parabolic form, since this is the lowest-order polynomial for which the cross-stream shear is nonzero. Let

$$\eta_0' = -\frac{\hat{\eta}_0'}{L_0^2}(L_0 - y)^2 \tag{32}$$

where L_0 is a cross-stream length scale which will be adjusted to fit the exponential profile, in order to facilitate comparison with the previous results. Substituting (32) in (15) gives

$$a'^2\left[1 + \frac{\hat{\eta}_0'}{hL_0^2}(L_0 - y)^2\right]v_{yy}' - \left[1 + \frac{2g'\hat{\eta}_0'}{f^2L_0^2}\right]v' = \frac{-\tau}{\rho f H}. \tag{33}$$

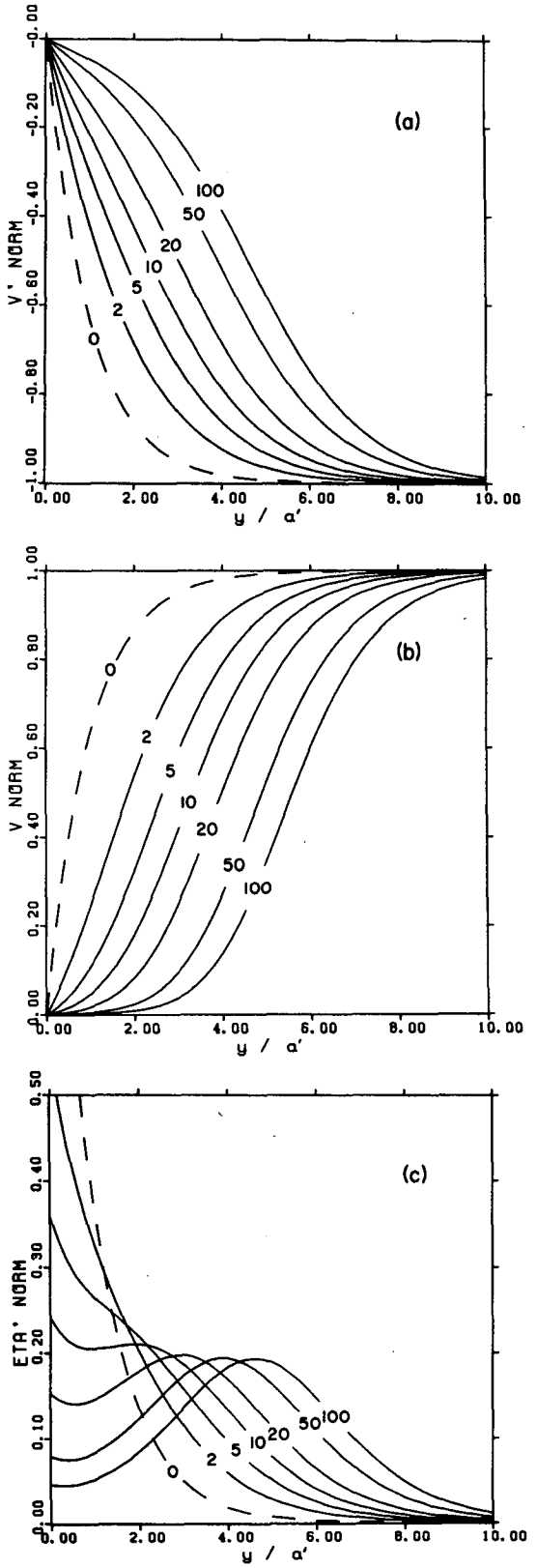

FIG. 4. Variations with a_* for exponential-profile jets: (a) v', (b) v, and (c) η', normalized as indicated in text.

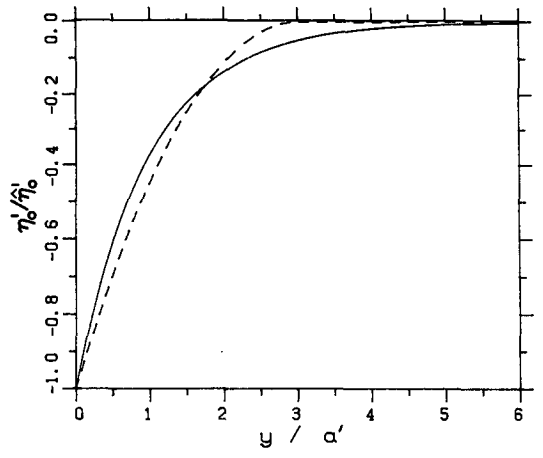

FIG. 5. Comparison of the exponential (solid line) and the parabolic (dashed line) forms of the interface (normalized as $\eta_0'/\hat{\eta}_0'$).

The solution is obtained by defining exterior ($y \geq L_0$) and interior ($y < L_0$) regions and requiring that v' and the interface be continuous across the boundary between these regions. In the exterior region, $\eta_0' = 0$ and

$$v_{ex}' = Ae^{-y/a'} + \frac{\tau}{\rho f H} \tag{34}$$

where A is a constant to be determined. Figure 5 shows that (32) provides a reasonable fit to the exponential shape when $L_0 = 3a'$. Defining a_* as before and $b_* \equiv (9 + 2a_*)$, and making the following change of variable,

$$\xi \equiv \sqrt{a_*}\left(1 - \frac{y}{L_0}\right), \tag{35}$$

(33) takes the form

$$(1 + \xi^2)v_{\xi\xi}' - \frac{b_*}{a_*}v' = \frac{-9\tau}{\rho f H a_*} \tag{36}$$

with $L_0 = 3a'$.

The solution to this equation can be expressed, for certain values of a_*, in terms of a sum of an infinite series and a Jacobi polynomial of order m. The former corresponds to $s = 1$ in (22), the latter to $s = 0$. The details are in the Appendix. The value of a_* depends upon the choice of m, and several possibilities are given in Table 1. We select a value applicable to a jet comparable to the Labrador Current. From (32) and the geostrophic relations for the upper layer, the maximum speed of the unperturbed jet at $y = 0$ is $\hat{u}_0 = \frac{2}{3}\sqrt{g'ha_*}$. Choosing $h = 100$ m and $\Delta\rho = 0.5$ kg m^{-3} (Fig. 1) gives a reasonable value for $\hat{u}_0$ (42 cm s^{-1}) with $a_* = 0.9$. From Table 1 we therefore select the $m = 2$ case, for which the solution for v' is

$$v_{in}' = \frac{\tau}{\rho f H}\frac{1}{6}\{B'(1 + 6\xi^2 + 5\xi^4) + C'\sum_{k=0}^{\infty} A_{2k+1}\xi^{2k+1} + 5\} \tag{37a}$$

$$v_{ex}' = \frac{\tau}{\rho f H}(1 + A'e^{-y/a'}) \tag{37b}$$

where $A' = -2.57036$, $B' = 0.232177$ and $C' = -2.42807$. The coefficients A_n are given in Table 2 up to $n = 15$, for n odd, together with the recursion relation. The convergence of the infinite series is discussed in the Appendix.

The velocity in the upper layer is found by using (10). Substitution of ξ from (35), and taking the limit $h'/h \gg 1 > \xi^2$ gives the interior solution

$$v_{in} = \frac{-h'}{h}\frac{1}{(1 + \xi^2)}v_{in}' \quad 0 \leq \xi \leq \sqrt{a_*}. \tag{38a}$$

The exterior solution for v is

$$v_{ex} = \frac{-h'}{h}v_{ex}'. \tag{38b}$$

Similarly from (8c) and (35) the displacement of the interface in the interior region is

$$\eta_{in}' = \frac{\tau t}{\rho f a'}\frac{h'}{H}\frac{\sqrt{0.9}}{18}(4B'(3\xi + 5\xi^3) + C'\sum_{k=0}^{\infty} A_{2k+1}\xi^{2k}), \tag{39a}$$

and the exterior solution is

$$\eta_{ex}' = \frac{\tau t}{\rho f a'}\frac{h'}{H}A'e^{-y/a'}, \quad y \geq L_0. \tag{39b}$$

The solutions for v', v and η', normalized as before, are shown in Fig. 6. These are to be compared with the results for the exponential profile with $a_* = 0.9$ in

TABLE 1. Parameters determining α_*.

m	α_*
1	∞
2	0.9
3	0.32
≥ 4	≤ 0.08

TABLE 2. The coefficients A_n for n odd. The recursion relation is $n(n-1)A_n + [(n-2)(n-3) - 12]A_{n-2} = 0$.

n	A_n
1	1
3	2
5	3/5
7	−4/35
9	1/21
11	−2/77
13	7/429
15	−8/715

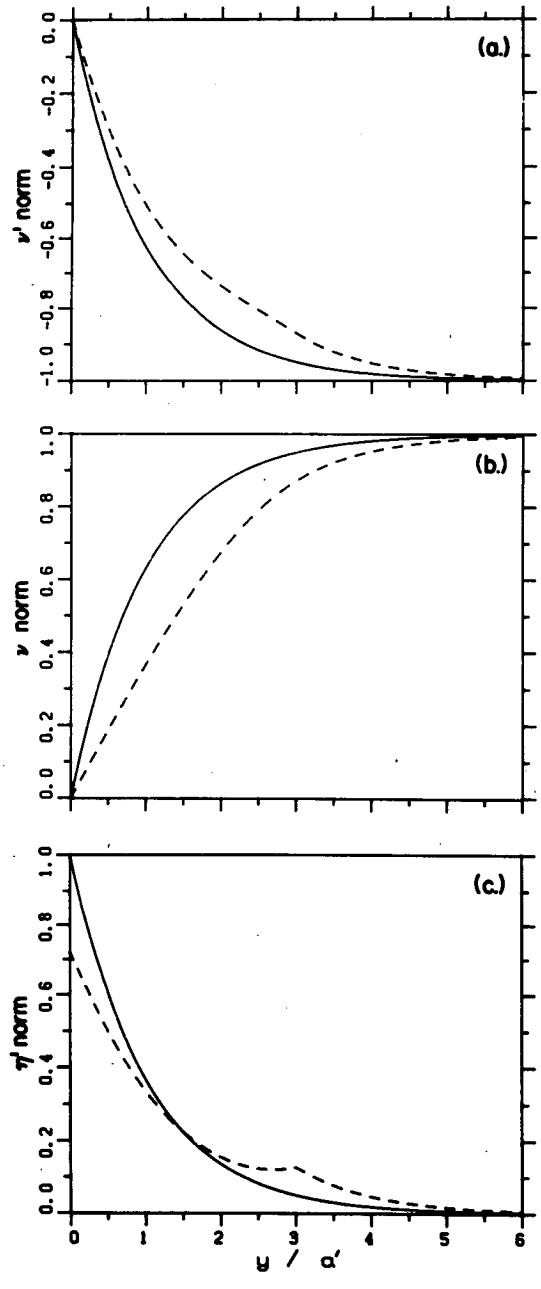

FIG. 6. Parabolic case. (a) Lower-layer velocities; (b) upper-layer velocities; and (c) interfacial displacements, normalized as indicated in the text. The solid line is the usual (no-jet) solution; the dashed line the solution in the presence of a jet.

Fig. 3. The two solutions display essentially the same features: reduced on–offshore flow everywhere in both layers near the coast, reduced upwelling rates for $y \leqslant a'$, and enhanced upwelling rates farther offshore. The only major difference occurs at $y = 3a'$, the boundary between the interior and exterior regions. In the parabolic case, however, a sharp maximum in upwelling rate occurs at this boundary. This maximum represents a stepwise change in $v'_{\gamma\gamma}$ and arises from the matching procedure at the boundary.

5. Barotropic response

It is necessary to revoke the rigid-lid approximation and convenient to rewrite (7) and (8) in the form

$$U_t - fV = \frac{\tau}{\rho} + \left(\frac{g'}{f}\eta'_{0yy}V\right) \tag{40a}$$

$$fU = -g(h - \eta'_0)\eta_y \tag{40b}$$

$$V_y = -\eta_t + \eta'_t \tag{40c}$$

$$U'_t - fV' = 0 \tag{41a}$$

$$fU' = -g(h' + \eta'_0)(\eta_y + \epsilon\eta'_y) \tag{41b}$$

$$V'_y = -\eta'_t \tag{41c}$$

where $U = (h - \eta'_0)u$, $U' = (h' + \eta'_0)u'$, and so on, and $\epsilon = (\rho' - \rho)/\rho$. We have dropped the V_t and V'_t terms because solutions in which the on–offshore motion is steady are sought.

We wish to find the governing equations for the barotropic mode. It can be shown in the no-jet case (e.g., Csanady 1982, pp. 83–91) that two uncoupled linear combinations of (40) and (41) exist, one for each of the barotropic and baroclinic modes. In the presence of a jet, however, this approach meets with difficulty because the multiplicative factors in the linear combination must in general be functions of y. We therefore adopt an alternate approach in which

$$\eta' = \alpha\eta. \tag{42}$$

Usually the proportionality factor α is taken to be constant (e.g., Gill 1982, p. 120), but here $\alpha = \alpha(y)$. The governing equations for the baroclinic mode may be recovered by taking $\alpha \gg 1$. This is equivalent to the rigid-lid approximation: (40) and (41) reduce to (7) and (8).

In the barotropic mode, however, we expect $\alpha \sim$ O(1). Since $\epsilon \ll 1$, the sum of (40) and (41) yields

$$(U + U')_t - f(V + V') = \frac{\tau}{\rho} + \left(\frac{g'}{f}\eta'_{0yy}V\right) \tag{43a}$$

$$f(U + U') = -gH\eta_y \tag{43b}$$

$$(V + V')_y = -\eta_t. \tag{43c}$$

These are the usual equations for the barotropic mode, except for the advective term on the right in (43a). Fortunately this term is small for the cases of interest here. That is, the Rossby number for the barotropic mode

$$\mathrm{Ro}_1 = \frac{g'}{f^2}\eta'_{0yy}\frac{V}{V + V'} \tag{44}$$

is small, as shown below.

We first consider the case of a weak jet: that is, one for which the Rossby number, even in the baroclinic mode, is small. The advective term in (43a) can then be safely ignored, and we have the usual results

$$(V + V') = \frac{\tau}{\rho f}(e^{-y/a} - 1) \tag{45}$$

$$\eta_t = \frac{\tau}{\rho f a} e^{-y/a} \tag{46}$$

where $a = \sqrt{gH}/f$ is the external Rossby radius. In order to find $V/(V + V')$, however, an expression for α is needed. Since in the absence of a jet α is just the fractional height of the interface above bottom (see Csanady 1982, p. 87), we choose

$$\eta' = \left(\frac{h' + \eta'_0}{H}\right)\eta. \tag{47}$$

Equation (41c) becomes

$$V'_y = -\left(\frac{h' + \eta'_0}{H}\right)\eta_t \tag{48}$$

which, for $|\eta'_0| \ll h'$, simplifies to

$$V' \approx \frac{h'}{H}\frac{\tau}{\rho f}(e^{-y/a} - 1). \tag{49}$$

Making use of (45), we find that

$$V \approx \frac{h}{H}\frac{\tau}{\rho f}(e^{-y/a} - 1), \tag{50}$$

and the Rossby number (44) becomes

$$\mathrm{Ro}_1 \approx \frac{h}{H}\left(\frac{g'\eta'_{0yy}}{f^2}\right). \tag{51}$$

It is seen that Ro_1 is $O(h/H)$ times the Rossby number for the baroclinic mode and that even if the latter is $O(1)$, $\mathrm{Ro}_1 \ll 1$ for $h \ll H$ (14b). In particular, for a jet profile given by (19),

$$\mathrm{Ro}_1 \approx \frac{|\eta'_0|}{H}$$

which, given (14a), is small. We conclude that the advective term does not contribute significantly to the momentum balance in the barotropic mode, and that the usual results (45) and (46) apply even in the presence of a jet, provided the conditions (14a) and (14b) are met.

6. Discussion and conclusions

Analytic solutions to the problem of steady upwelling in the presence of a coastally trapped upper-layer jet have been obtained for the cases in which the cross-stream equilibrium profile of the interface is either exponential or parabolic. It is also shown that solutions should be obtainable when the jet profile can be expressed as a polynomial in the offshore coordinate. The exponential case corresponds to a frictionless jet in geostrophic balance with potential vorticity uniform in the cross-stream direction. The parabolic profile is adjusted to approximate the exponential. The solutions apply when both the upper-layer thickness and the equilibrium displacement of the interface are much less than the lower-layer thickness.

The barotropic response is unaffected by the jet, essentially because the requirement that the upper layer be thin results in the nonlinear advective term being unimportant. This occurs by virtue of the fact that the on–offshore velocities are approximately equal in each layer in this mode, and therefore the Rossby number involving the on–offshore volume transports is small.

The baroclinic response, on the other hand, is considerably modified. Upwelling rates are reduced at the coast and enhanced at offshore distances greater than the internal deformation radius. For a jet with a (baroclinic) Rossby number of unity, the degree to which the response is modified depends on the speed of the jet at the coast. For high-speed jets upwelling at the coast is almost entirely suppressed, and a second upwelling zone develops offshore beyond $y = a'$.

The physical mechanism behind the modified upwelling response can be understood in terms of the divergence of the on–offshore velocities in each layer. In section 4 we showed that as in the no-jet case, it is this divergence which drives the vertical displacements. In the presence of a jet the divergence is reduced at the coast, and with increasing jet speed at constant cross-stream scale the position of the zone of maximum divergence moves offshore. This occurs as a consequence of three effects. First, in the vertically integrated equations of motion, the wind stress is applied to an upper layer that is thickest at the coast [Eq. (7a)]. Second, the presence of the interface sloping downward toward the coast imposes a constraint on the on–offshore motion through the continuity equation which results in increased divergence of this motion at points immediately offshore. Third, the nonlinear term in the alongshore momentum equation (7a) can be considered to cause a change (in this case an increase) in the effective Coriolis parameter, as suggested by Niiler (1969). Such a reduction would result in decreased offshore Ekman transport in the upper layer. The modified response is the net result of all three effects, however, and we have retained the unmodified Coriolis parameter in the definition of the Rossby radius, which remains the natural offshore length scale for the problem even in the presence of a jet. Examining (20), or its alternate (15), there is no obvious way in which a modified parameter can be defined which would reduce this to the usual no-jet form. For an exponential-profile jet, however, it is clear from (20) that the net effect can be thought of as either a reduction in the effective wind stress or an increased effective depth.

Finally we note that of the jets considered here, the slower-speed ones will in general be more readily realized in the ocean. The parameter a_* [see Eq. (26)] is, for the exponential-profile jets with the form (19), just the jet Rossby number at the coast. Jets corresponding to values of this parameter much greater than unity are considered here in order to illustrate the tendency for the zone of maximum divergence to shift offshore.

In summary, we have extended the usual two-layer upwelling problem to include a coastally trapped upper-layer jet. By linearizing the governing equations through a perturbation expansion of the displacement and velocity fields, analytic solutions are obtained. The principal differences between these results and the usual ones for the no-jet case are that upwelling is reduced at the coast and amplified offshore. The differences are due to a reduction in the divergence of the on–offshore velocities within an internal Rossby radius of the coast and to increased divergence farther offshore. These changes in divergence are the result of the equilibrium displacement of the interface through the continuity equation and of advection of mean-flow momentum by wind-induced offshore motion through the cross-stream shear.

Acknowledgments. This work was funded by Grant A8846 from the Natural Sciences and Engineering Research Council, Canada. We thank John Anderson, Northwest Atlantic Fisheries Centre, for making the data in Fig. 1 available to us.

APPENDIX

Series Solution for the Baroclinic Mode with a Parabolic Profile

The homogeneous equation for the interior is, from (36),

$$(1 + \xi^2)v'_{\xi\xi} - \frac{b_*}{a_*} v' = 0, \quad 0 \leqslant \xi \leqslant \sqrt{a_*}. \quad \text{(A1)}$$

A further change of variable $\chi \equiv -\xi^2$ gives

$$\chi(1 - \chi)v'_{\chi\chi} + \left(\frac{1}{2} - \frac{\chi}{2}\right)v'_\chi + \frac{b_*}{4a_*} v' = 0,$$

$$-a_* \leqslant \chi \leqslant 0. \quad \text{(A2)}$$

A standard solution to (A2) in terms of Jacobi polynomials exists when

$$\frac{b_*}{2a_*} = m(2m - 1) = N$$

where m is a positive integer. Therefore,

$$a_* = \frac{\hat{\eta}'_0}{h} = \frac{9}{2(N - 1)}. \quad \text{(A3)}$$

As discussed in the text, only the $m = 2$ case is considered. Returning now to (A2), the solution for $m = 2$ is the second-order Jacobi polynomial

$$J_2\left(\frac{1}{2}, \frac{-1}{2}, -\chi\right) = 1 + 6\chi + 5\chi^2, \quad |\chi| < 1. \quad \text{(A4)}$$

This does not represent the complete solution, however. Using the values above, (A1) becomes

$$(1 + \xi^2)v'_{\xi\xi} - 12v' = 0. \quad \text{(A5)}$$

The substitution

$$v' = \sum_{k=0}^{\infty} A_k \xi^{k+s}$$

using the method of Frobenius yields two independent solutions:

for $s = 0$,

$$v'_1 = A_0 + A_2\xi^2 + A_4\xi^4 \quad \text{(A6a)}$$

for $s = 1$

$$v'_2 = A_1\xi + A_3\xi^3 + A_5\xi^5 + A_7\xi^7 + \cdots. \quad \text{(A6b)}$$

The coefficients A_n are given in Table 2 up to $n = 15$, for n odd, together with the recursion relation. The values: $A_0 = 1$, $A_2 = 6$, $A_4 = 5$, and $A_{n\geqslant 6} = 0$ (for even n), are the same as the coefficients of $J_2(1/2, -1/2, -\chi)$.

Now, from (36), with $a_* = 0.9$, the particular solution for the interior is

$$v'_p = \frac{5}{6}\frac{\tau}{\rho f H}. \quad \text{(A7)}$$

The complete solution in the interior is therefore

$$v'_{\text{in}} = Bv'_1 + Cv'_2 + v'_p \quad \text{(A8)}$$

where B and C are constants to be determined.

The boundary conditions are that $v'_{\text{in}} = 0$ at the coast and that v' and η' (or equivalently v'_y by 7c and 8c) be continuous at $y = L_0$. Therefore,

$$10.4500B + 3.0585C + \frac{5}{6}\frac{\tau}{\rho f H} = 0 \quad \text{(A9)}$$

at $y = 0$. Continuity of velocity at $y = L_0$ requires that

$$B = Ae^{-3} + \frac{1}{6}\frac{\tau}{\rho f H}, \quad \text{(A10)}$$

$$C = \frac{3A}{\sqrt{a_*}} e^{-3} \quad \text{(A11)}$$

because v'_y is continuous at $y = L_0$. These equations are solved for A, B and C, yielding the final result, Eqs. (37).

The convergence of the infinite series in the interior solutions (37a) and (38a) was investigated. Because $0 \leqslant \xi < 1$ everywhere, the most stringent test is at the coast where $\xi = \sqrt{0.9}$. Depending upon the accuracy desired, the solutions converge quite rapidly at the coast

largely because of the comparatively high values of the leading terms in the series (Table 2). For example, letting n represent the highest power of ξ in the nth-order partial sum, v'_{in} (37a normalized by $\tau/\rho fH$) is within 0.4% of zero for the 9th-order partial sum. Because consecutive terms in the C' series alternate in sign for $n \geq 7$ and are of nearly equal value, the rate of convergence of the higher-order partial sums is rather slow. Advantage can be taken of this, however. The arithmetic average of consecutive pairs of partial sums approaches the limit quite rapidly: the average of the 9th- and 11th-order partial sums is within 0.01% of zero, whereas the 15th-order partial sum must be computed to obtain equal accuracy. The same remarks apply to the result for η'_{in} (40a): the 9th-order partial sum differs by 1.8% from the true limit; the average of the 7th and 9th order partial sums by only -0.7%. To obtain equal accuracy, the 15th-order partial sum must be computed.

REFERENCES

Csanady, G. T., 1982: *Circulation in the Coastal Ocean.* Reidel, 279 pp.

Gill, A. E., 1982: *Atmosphere-Ocean Dynamics. Int. Geophys. Ser.*, Vol. 30, William L. Donn, Ed., Academic Press, 662 pp.

Griffiths, R. W., P. D. Killworth and M. E. Stern, 1982: Ageostrophic instability of ocean currents. *J. Fluid Mech.* **117**, 343–377.

Hildebrand, F. B., 1962: *Advanced Calculus for Applications.* Prentice-Hall, 646 pp.

Hill, H. W., P. G. W. Jones, J. W. Ramster and A. R. Folkard, 1975: The current system east of Newfoundland Grand Bank. Int. Comm. Northwest Atlantic Fisheries, Spec. Pub. 10, 41–55.

Niiler, P. P., 1969: On the Ekman divergence in an oceanic jet. *J. Geophys. Res.*, **74**, 7048–7052.

Petrie, B., and C. Anderson, 1983: Circulation on the Newfoundland continental shelf. *Atmos. Ocean,* **21**, 207–226.

Smith, E. H., F. M. Soule and O. Mosby, 1937: The *Marion* and *General Greene* expeditions to Davis Strait and Labrador Sea. *Bull. U.S. Coast Guard,* No. 19, 259 pp.

Stommel, H., 1965: *The Gulf Stream.* University of California Press, 248 pp.